npg

BCLAF1 is a radiation-induced H2AX-interacting partner involved in γH2AX-mediated regulation of apoptosis and DNA repair

YY Lee[1], YB Yu[1,3,4], HP Gunawardena[1,3], L Xie[1] and X Chen*[1,2,3,4]

H2AX, a histone H2A variant, has a key role in the cellular response to DNA double-strand breaks (DSBs). H2AX senses DSBs through rapid serine 139 phosphorylation, concurrently leading to the formation of phospho-(γ)H2AX foci with various proteins. However, in the cells with different sensitivity to ionizing radiation (IR)-induced DSBs, still incomplete are those specific proteins selectively recruited by γH2AX to decide different cell fates. Because the abundance of γH2AX indicates the extent of DSBs, we first identified IR-induced dose-dependent H2AX-interacting partners and found that Bcl-2-associated transcription factor 1 (BCLAF1/Btf) showed enhanced association with γH2AX only under high-dose radiation. In acutely irradiated cells, BCLAF1 promoted apoptosis of irreparable cells through disturbing p21-mediated inhibition of Caspase/cyclin E-dependent, mitochondrial-mediated pathways. Meanwhile, BCLAF1 co-localized with γH2AX foci in nuclei and stabilized the Ku70/DNA-PKcs complex therein, facilitating non-homologous end joining (NHEJ)-based DSB repair in surviving cells. In tumor cells, BCLAF1 was intrinsically suppressed, leading to formation of anti-apoptotic Ku70–Bax complexes and disruption of Ku70/DNA-PKcs complexes, all of which contribute to tumor-associated apoptotic resistance and cell survival with defective NHEJ DNA repair. For the first time, our studies reveal that, based on the extent of DNA damage, BCLAF1 is involved in the γH2AX-mediated regulation of apoptosis and DNA repair, and is a γH2AX-interacting tumor suppressor.

Based on the severity of DNA damage, cells activate specific pathways for cell fate decisions. While an acute ionizing radiation (IR) triggers pro-apoptotic signals in cells with irreparable DNA damage,[1] cells persistently exposed to radiation can become resistant/adapted to double-strand breaks (DSBs),[2] which are with an increased risk of carcinogenesis. However, the pathways/mechanisms that determine defined cell fate remain to be elucidated.

The replacement histone H2AX senses DSBs with rapid phosphorylation of serine 139 (γH2AX), which recruits various proteins associated with DNA damage/repair, cell cycle check points,[3] and so on, to form γH2AX foci indicative of DSB-associated genome instability[4] and premalignant lesions.[3] By using our quantitative proteomics approach,[5,6] we have identified novel H2AX-associating proteins, revealing new aspects of H2AX in regulating IR-induced cell cycle arrest[7] and nucleosome dynamics.[8] Together with recent findings that changes in H2AX site-specific phosphorylation[9] can selectively modulate cellular apoptosis or survival,[10] we reasoned that H2AX coordinates a post-DSB 'switching' program that chooses specific cell fate-determining pathways

by selectively recruiting particular proteins in the cells differentially irradiated with acute *versus* prolonged IR.

By multiplex quantitative proteomics,[7] we first examined how different H2AX-coordinated complexes are formed in cells exposed to different IR doses. We found the most notable hierarchical clusters of high-dose IR-induced γH2AX interactors were those associated with p53 regulation, apoptosis, or both, among which was BCLAF1, previously implicated in TP53-mediated DDR/apoptosis,[11] and lung development.[12] We then explored the novel function of BCLAF1 in the γH2AX-coordinated cell fate-determining pathways under different radiation conditions including those diverse phenotypes associated with either induction of apoptosis in irreparable cells, or cell survival with active DNA repair, or cell survival toward carcinogenesis. From a systemic viewpoint, for the first time, we have elucidated a mechanistic link between the γH2AX-mediated interaction network and different cell fate-determining pathways that drive cells toward either survival or carcinogenesis following exposure to acute or prolonged IR. Specifically, we revealed how dysregulated BCLAF1 under radio-resistant conditions is associated with an impaired apoptotic feedback loop and ineffective DNA repair.

[1]Department of Biochemistry and Biophysics, University of North Carolina at Chapel Hill, Chapel Hill, NC 27599, USA; [2]Lineberger Comprehensive Cancer Center, University of North Carolina at Chapel Hill, Chapel Hill, NC 27599, USA; [3]Center for Technology Development of Proteomics, University of North Carolina at Chapel Hill, Chapel Hill, NC 27599, USA and [4]Department of Chemistry, Fudan University, Shanghai, China
*Corresponding author: X Chen, Department of Biochemistry and Biophysics, Campus Box 7260, 120 Mason Farm Road, No. 3010 Genetic Medicine Building, Chapel Hill, NC 27599, USA. Tel: 919 843-5310; Fax: 919 966-2852; E-mail: xianc@email.unc.edu

Results

High-dose IR triggers the recruitment of various proteins associated with apoptosis and p53 regulation to γH2AX foci. Using our AACT-based quantitative proteomic approach[7] (Figure 1a), we unambiguously identified multiple IR-induced dose-dependent γH2AX-associating proteins (Supplementary Tables S1 and S2 and Supplementary Figure S1). We then performed a domain-based analysis to construct a two-dimensional hierarchical clustering map, wherein many IR-inducible γH2AX-associating proteins grouped either structurally or functionally, further confirming the accuracy of our proteomics data (Supplementary Tables S2 and S3 and Supplementary Figure S2). Meanwhile, the data-dependent network analysis[13] of the γH2AX interactome revealed connectivity among multiple proteins known to be associated with either regulation of p53,[14] cell cycle, or apoptosis[15] (Supplementary Figure S3 and Supplementary Table S2), suggesting that all of the pathways represented by these γH2AX-docking proteins are interconnected. It caught our special attention that among them, a pro-apoptotic p53 regulator, BCLAF1,[16] previously unknown to interact with H2AX, exhibited enhanced association with H2AX specifically in high-dose-irradiated cells (Figure 1b). Further, more BCLAF1 was detected in the γH2AX immunoprecipitate pulled down from 10-Gy-irradiated cells compared with those in low-dose or non-irradiated cells, which is consistent with the high-dose-induced increase of γH2AX population in the 'reverse-order' immunoprecipitate pulled down by using anti-BCLAF1 antibody (Figure 1c), indicating that BCLAF1 directly binds γH2AX in a high-dose IR-inducible manner.

High-dose IR triggers the translocation of BCLAF1 to γH2AX foci and an enhanced binding of BCLAF1 to CPE-TP53. Since an apoptotic signal can induce binding of BCLAF1 to a nuclear membrane protein, Emerin,[17] we used immunofluorescence to determine where this high-dose-dependent BCLAF1–γH2AX association occurs *in situ*. In non-irradiated cells, BCLAF1 was distributed widely in the nucleoplasm, clearly separated from the background γH2AX foci. In response to low-dose radiation, few BCLAF1 foci were induced close to the nuclei where γH2AX foci were also located. In the 10-Gy-irradiated pro-apoptotic cells showing significant chromatin condensation (Figure 1d), more BCLAF1 were co-localized with γH2AX foci close to the nuclear periphery where heterochromatin is located for coordinating either transcriptional regulation or maintenance of chromosome integrity.[18]

We next determined whether BCLAF1 is indeed involved in the γH2AX-mediated DSB damage recognition and repair. First, few BCLAF1 and 53BP1 were found co-localized in the 10-Gy-irradiated cells showing a significant chromatin condensation (Figure 1d), indicating that the dose-dependent translocation of BCLAF1 is highly sensitive to the extent of DSBs and is directly involved in γH2AX-mediated DNA damage response (DDR). Further, in chromatin immunoprecipitation analysis, binding of both BCLAF1 and γH2AX to CPE-TP53 was induced substantially in the 10-Gy-irradiated cells compared with non-treated cells (Figure 2a). Given BCLAF1 was previously known to positively regulate p53 expression by interacting CPE-TP53 during DNA damage,[11] these observations indicated that γH2AX in the nucleosome, accumulated at DNA damage sites, serves as the scaffold to temporarily assist BCLAF1, a pro-apoptotic transcriptional factor, to get access to CPE-TP53, leading to upregulated p53 mRNA and protein levels in the 10-Gy-irradiated cells (Figure 2b).

BCLAF1 is involved in p21-dependent cell cycle regulation. p53 is essential in diverse DDR pathways associated with either cell cycle arrest, DNA lesion repair, or induction of apoptosis in cells containing irreparable DNA damage.[14] Specifically, in cell cycle arrest at G_1 phase, p53 enhances transcription of $p21^{(cip1/waf1)}$, which in turn inhibits cdk activity.[14] Given the involvement of H2AX in the p53/p21 pathway[19] and the γH2AX-dependence of BCLAF1, we therefore explored the role of BCLAF1 in p53/p21-dependent cell cycle regulation by first examining the effect of BCLAF1 knockdown on expression of p53 and p21. As p53 expression is affected by SV40 large T-antigen present in the 293 T cells in which BCLAF1–H2AX interaction was first identified by proteomics (Figure 1b), we also studied the effect of short-interfering RNA (siRNA)-mediated knockdown of endogenous BCLAF1 in other cell lines of normal human fibroblasts (MRC-5 and WI-38), and human osteosarcoma (U2OS), respectively. As shown in Figure 2c, knocking down BCLAF1 slightly attenuated p53 expression in non-irradiated cells and had little effect on the 10-Gy IR-induced p53, but generally led to significant increases in p21 expression in these cell lines, suggesting that BCLAF1 is involved in p21 regulation.

We therefore tested whether BCLAF1 is required for p21-induced cell cycle arrest. In asynchronously growing MRC-5 cells highlighted by the phase-characteristic staining (Figures 2d and e), a pronounced G_1 phase accumulation was found, especially in the 10-Gy-irradiated cells with siRNA-mediated BCLAF1 knockdown, while without siRNA treatment the population of G_2/M phase cells decreased from 25% to 10%

Figure 1 Proteomic identification of IR-induced dose-dependent γH2AX-interacting partners including BCLAF1. (**a**) Workflow of AACT-based multiplex dual-tagging quantitative proteomic approach. The 293T cells stably expressing FLAG-tagged H2AX grown in either $^{12}C_6$-arginine (L), or $^{13}C_6$-arginine (M), or $^{13}C_6^{15}N_4$-arginine (H)-containing medium were subjected to IR at the dose level of 0, 7.5 cGy, and 10 Gy, respectively. The immunoprecipitates (IP) originated from each of the three cell pools were mixed at 1 : 1 : 1 ratio based on the amount of FLAG-tagged H2AX in each IP elute as measured by immunoblotting (IB) prior to mixing. The equally combined IP elutes were then separated by SDS-PAGE, digested with trypsin, and analyzed by nanoLC-MS/MS. (**b**) MS spectra of AACT-containing peptides of the representative proteins detected in the IP mixture. Peptide sequences include IDISPSTLR (BCLAF1), SILQER (Ku86), SDSFENPVLQQHFR (Ku70), LLEEALLR (DNA-PKcs). The relative abundance of the bait protein, H2AX, in each immunoprecipitate, was measured based on the ratio of isotope peak intensity, and the ratio was calibrated to 1 : 1 : 1 for the normalization of those of other H2AX-interacting proteins. (**c**) Immunoblot analysis of the immunoprecipitates pulled down from non-irradiated or 7.5-cGy- or 10-Gy-irradiated cells by anti-γH2AX antibody. A mouse IgG was used as the control. (**d**) Immunofluorescence analysis of IR dose-dependent BCLAF1-γH2AX association *in situ*. The 293T cells were irradiated at indicated dose level and were then incubated for 1 h prior to fixing and staining with indicated antibodies (lower panel) with both anti-mouse and -rabbit IgG antibodies as the control. 4,6-diamidino-2-phenylindole (DAPI) was used for DNA staining (top panel). The scale bar is 24 μm
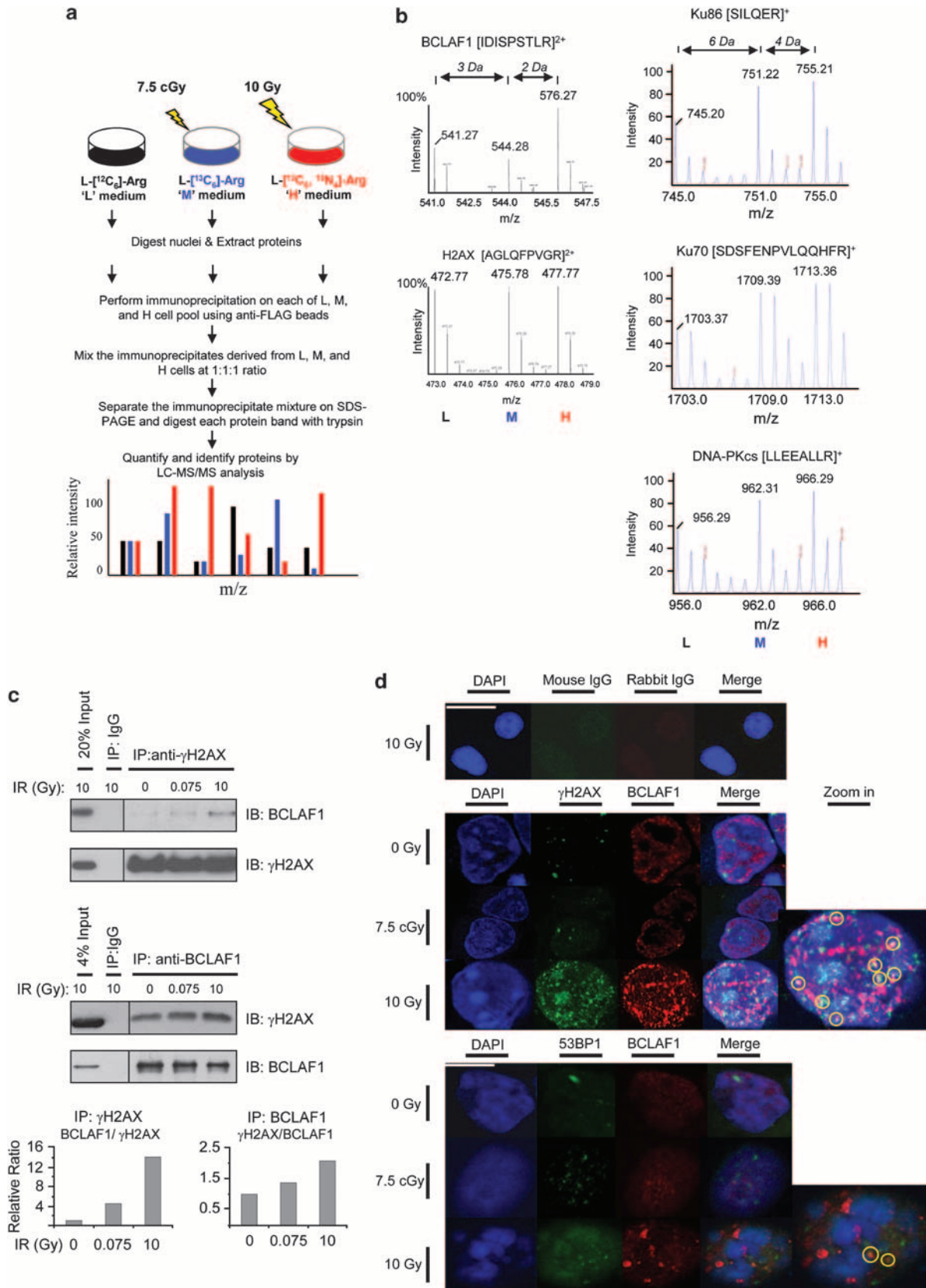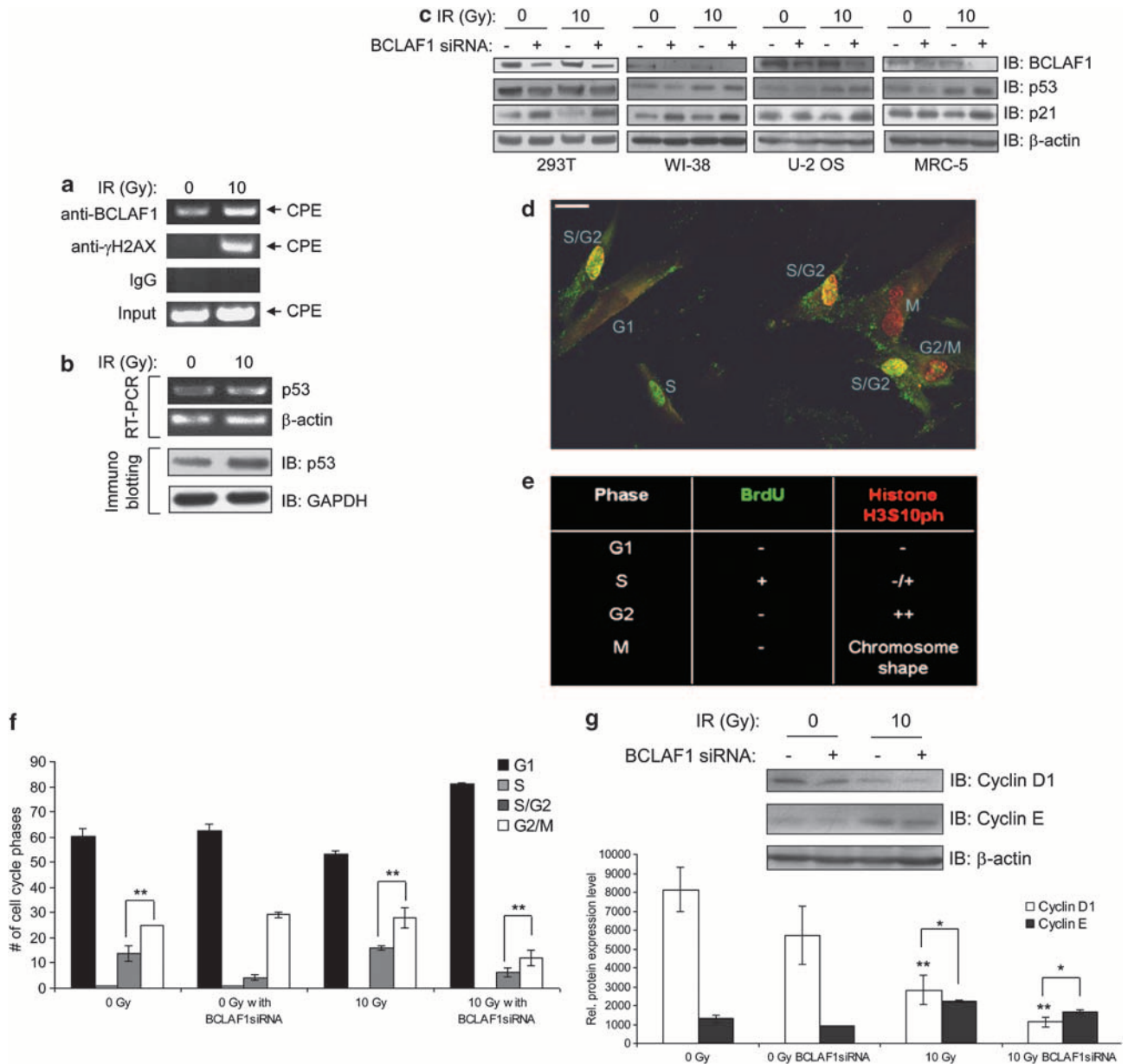
Figure 2 BCLAF1 is involved in the γH2AX-mediated regulation of p53/p21 expression and cell cycle progression. (**a**) Chromatin immunoprecipitation (ChIP) experiments were performed on non- or 10-Gy-irradiated cells by using anti-BCLAF1 or anti-γH2AX antibody, respectively. The amount of CPE-TP53 bound to either BCLAF1 or γH2AX in the immunoprecipitate was assayed by RT-PCR using the primers as previously described[11] with IgG and input as the quantitative controls. (**b**) Total RNA was extracted from non- or 10-Gy-irradiated cells and analyzed by RT-PCR using the primers specific for each of p53 and β-actin. The cell lysates were also immunoblotted (IB) against p53 antibody with GAPDH as the control. (**c**) The expressions levels of p53 and p21 were compared in four different cell lines including 293T, WI-38, U-2 OS, and MRC-5 without or with siRNA-mediated BCLAF1 knockdown. Immunoblotting experiments were performed with the indicated antibodies with β-actin as the loading control. (**d**) Immunostaining analysis of different phases of cell cycle of MRC-5 cells. BrdU (green) labels S-phase cells while the staining in red for serine 10 phosphorylation at histone H3 (H3S10ph) highlights the cells at G_2/M phase. The cells at either G_1- or G_2/M-phase were distinguished by either no staining or relatively intense staining, respectively. The co-staining cells were at S/G_2 or late S phase while M-phase cells were identified by their unique chromosomal shape following DAPI staining for DNA (blue). Different cell cycle phases are indicated in light blue. The scale bars represent 10 μm. (**e**) Distribution of cell cycle phases highlighted by BrdU and Histone H3S10ph staining. (**f**) BCLAF1 effect on IR-induced cell cycle progression. The percentages of MRC-5 cells without or with 10 Gy IR at each different cell cycle stage, G_1, S, S/G_2, and G_2/M, were measured by BrdU and H3S10ph staining and compared with those in the cells with siRNA-mediated BCLAF1 knockdown (BCLAF1 si). One experiment containing a technical duplicate representative of two is shown with the data precision indicated by the error bar based on mean ± S.D. of duplicate samples. **$P < 0.05$. (**g**) Effect of BCLAF1 knockdown on the expression of cyclin D1 and cyclin E. MRC-5 cells were transfected with BCLAF1 siRNA for 2 days prior to immunoblot analysis of the cyclins with indicated antibodies at 1 h after the radiation. β-actin was used as the loading control (upper panel). The intensity of each gel band was determined by ImageJ software. One experiment containing a technical duplicate representative of two is shown with the data precision indicated by the error bar based on mean ± S.D. of duplicate samples. **$P < 0.05$, *$P < 0.01$

(Figure 2f). Together with the result (Figure 2c), the suppression of BCLAF1 promotes both a p21 upregulation and a p21-dependent growth arrest in G_1.

In a p21-dependent manner, cyclin D1 and E are known as the essential components for regulating the cell cycle at either early G_1 or for late G_1-to-S transition.[20] Because BCLAF1 was

found in a complex that regulates cyclin D1 mRNA stability,[21] we tested if BCLAF1 could regulate the p21-dependent cyclin D1 and E. In the 10-Gy-irradatied cells, cyclin D1 was downregulated, while cyclin E was upregulated. siRNA-mediated BCLAF1 knockdown then suppressed more cyclin D1 than that of cyclin E in cells with or without IR (Figure 2g), indicating that BCLAF1 affects cell cycle progression by regulating the p21-dependent cyclins in early G_1, which is often dysregulated in human cancers.[22]

BCLAF1 is suppressed in radio-resistant cells, and BCLAF1 differentially regulates cyclin E-mediated cell cycle progression in differently irradiated cells. Further, we clarified how BCLAF1 regulates diverse DDR to different extents of DNA damage in either non-irradiated cells, or IR-responsive cells irradiated by a high-dose radiation at 10 Gy,

and IR-adapted/-resistant cells, which were first primed with 7.5 cGy for 24 h before a second high-dose radiation at 10 Gy (Figure 3a). These cells under each radiation condition were collected at a single time point with 1 h post irradiation recovery. We observed that the 10-Gy IR-responsive cells displayed a higher propensity for apoptosis indicated by intense DNA fragmentation, whereas the IR-adapted cells were radio-resistant/pro-survival and characterized by significantly reduced DNA fragmentation (Figure 3a). Because BCLAF1 was found linking to either pulmonary smooth muscle development[23] or tumor suppression,[12] both wild-type p53 human adenocarcinoma A549 cells[16] and p53-deficient lung carcinoma H1299 cells[24] were chosen. Compared with its expression in IR-responsive A549 cells, BCLAF1 was found to be intrinsically suppressed under IR-resistant condition with simultaneously induced p53 and p21
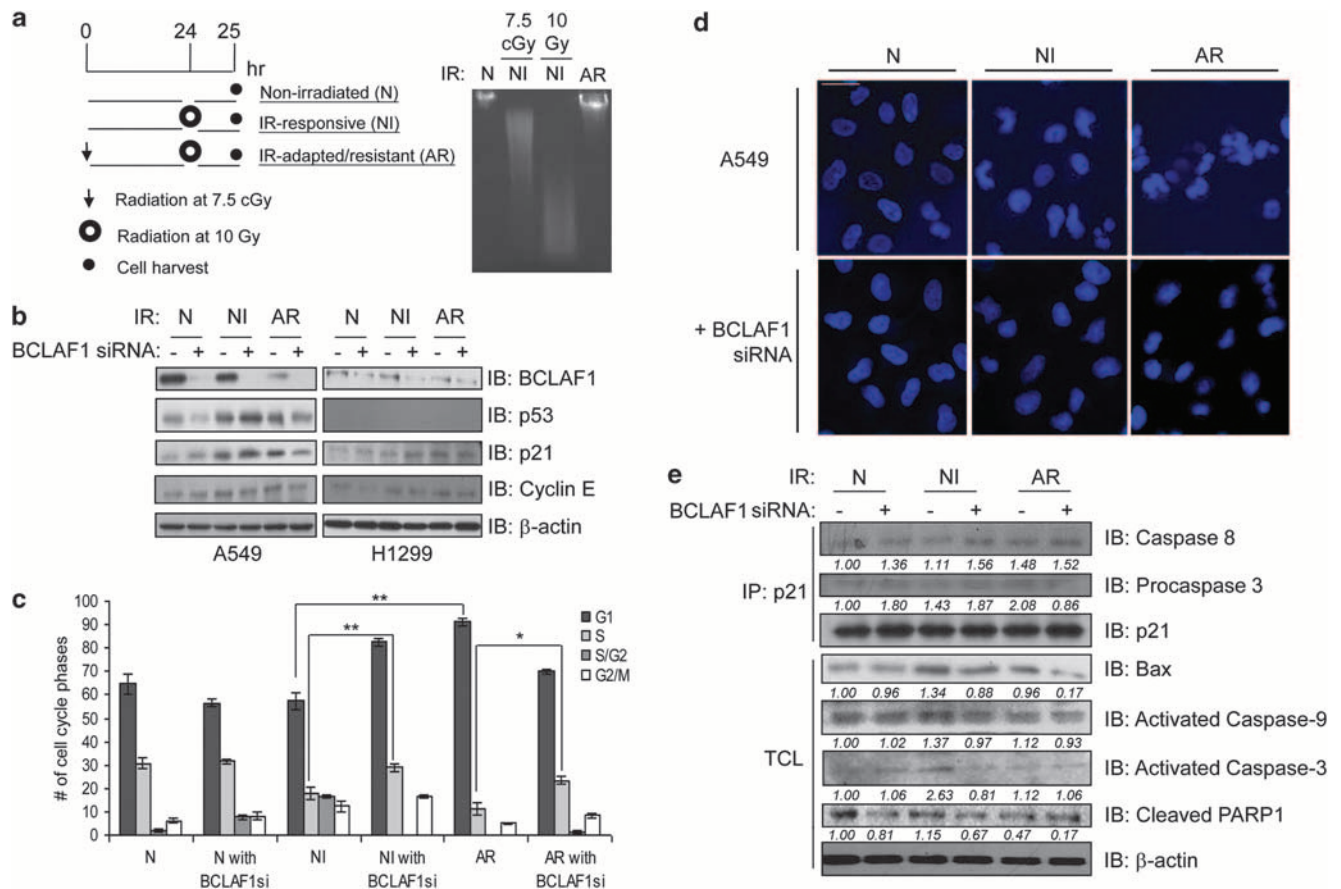

Figure 3 BCLAF1 differentially regulates p21-mediated G1 arrest and apoptotic activity in differentially irradiated cells. (**a**) Schematic design for generating either 'IR-responsive or pro-apoptotic' or 'IR-resistant/-adapted or pro-survival' cells from their exposure to a high-dose (10 Gy) radiation either without or with a 24-h priming IR at low dose (7.5 cGy), respectively. (**b**) Immunoblot analysis of the effect of BCLAF1 knockdown by siRNA on expression of p53, p21, and cyclin E in differentially irradiated A549 and H1299 cells. β-actin was used as the loading control. (**c**) Effect of BCLAF1 on the cell cycle progression of differentially irradiated cells. The percentages of different cell cycle phases including G_1, S, S/G_2 and G_2/M were compared for non-irradiated, IR-responsive, and IR-resistant A549 cells without or with siRNA-mediated BCLAF1 knockdown (BCLAF1 si). One experiment containing a technical duplicate representative of two is shown with the data precision indicated by the error bar based on mean ± S.D. of duplicate samples. **$P < 0.05$, *$P < 0.01$. (**d**) Effect of BCLAF1 knockdown on the growth and morphology of differentially irradiated A549 cells. DAPI was used to stain DNA. The scale bar is 48 μm. (**e**) Effect of BCLAF1 knockdown on p21 association with caspase 8 and procaspase-3. Immunoblotting analysis was conducted on the p21 immunoprecipitates from each set of the differentially irradiated A549 cells without or with siRNA-mediated BCLAF1 knockdown (upper panel). Also the levels of Caspase-9, Caspase-3, and cleaved PARP-1 in whole cell lysates of these untreated or treated cells were analyzed by immunoblotting with indicated antibodies. β-actin was used as the loading control (bottom panel). Relative intensities representing the binding strength between p21 and either Caspase 8 or Procaspase 3 as well as the expression of Bax, activated Caspase-9, activated Caspase-3, and cleaved PARP1 in total cell lysate (TCL) were measured by ImageJ (version 1.4.5q) and are indicated as italic numbers. Data shown are from two independent experiments. $P < 0.01$

(Figure 3b). siRNA-mediated BCLAF1 knockdown (Supplementary Figure 4) also led to similarly increased expression of p53 and p21 but slightly decreased cyclin E in the IR-responsive cells. However, in the same type of A549 cells under IR-resistant condition, siRNA depletion of BCLAF1 correlated with suppressed expression for p53, p21, and cyclin E. Also, compared with IR-responsive cells, the level of cyclin E, which was generally decreased with siRNA knockdown of BCLAF1, showed an increase in the IR-resistant A549 cells having already suppressed BCLAF1 (Figure 3b). Interestingly, in p53-deficient H1299 cells, both activated p21 and reduced cyclin E were accompanied with reduced BCLAF1 either under IR-resistant condition or siRNA BCLAF1 knockdown (Figure 3b), collectively indicating that in a p53-independent but p21-dependent manner, BCLAF1 differentially regulates the cyclin E-mediated pathways at G_1/S phase based on the IR-responsive or -resistant nature of the cells.

BCLAF1 negatively regulates the p21-dependent cell cycle arrest in a H2AX-dependent manner. Next, we investigated exactly how BCLAF1 affects the p21-dependent cell cycle in the differentially irradiated cells. First, 82% of the IR-responsive cells with BCLAF1 knockdown, and 91 or 70% of IR-resistant cells without or with BCLAF1 knockdown were retained in G_1, compared with 60% G_1 retention observed for non-irradiated or other types of irradiated cells (Figure 3c). This pronounced G_1 retention associated with either siRNA-mediated knockdown or IR-resistant downregulation of BCLAF1 was concomitant with an increase of p21 (Figure 3b). Further, in the irradiated cells, BCLAF1 knockdown led to an approximately two-fold increase of S-phase cells coincident with a reduction of cyclin E, which is generally downregulated in S phase (Figures 3b and c). Also, in the immunofluorescence analysis of radiation effect on the growth of wild-type A549 cells, we found that the high-dose IR-induced chromatin condensation occurred only in IR-responsive cells, indicating their pro-apoptotic nature (Figure 3d and Supplementary Figure S5). In contrast, under IR-resistant condition we found these cells not only formed the multicellular spheroids characteristic of radio-resistance[25] but also were accumulated more at G1 showing another radio-resistant character[26] (Figures 3c and d). Intriguingly, no apparent condensed chromatin was observed in the IR-responsive cells with BCLAF1 knockdown. Further, all types of the cells with BCLAF1 knockdown became widely

distributed in a separate manner, and larger cell populations were observed at S phase.[26] This phenomenon of separated distribution was more pronounced in the BCLAF1 knockdown cells under IR-adapted conditions (Figures 3c and d). Taken together, BCLAF1 is a negative regulator of p21-dependent cell cycle arrest at either G1 or S phase and inhibits a pro-survival-characteristic distribution of the cell population.

In addition to promoting cell cycle arrest, activated p21 was also known to inhibit apoptosis by suppressing the activation of Caspase 8 and pro-Caspase 3.[27] We therefore investigated whether BCLAF1 affects the activation of Caspase 8 and pro-Caspase 3 by examining the p21 complexes immunoprecipitated from differentially irradiated A549 cells without or with BCLAF1 knockdown (Figure 3e). Stronger associations between p21 and Caspase 8 or pro-Caspase 3 were observed in either IR-resistant cells or the irradiated cells with BCLAF1 knockdown, indicating reduced levels of BCLAF1, either naturally in radio-resistant cells or by siRNA, are required for p21-mediated inhibition of Caspase-dependent apoptosis. Further, in line with previous evidence that overexpression of BCLAF1 induces a pro-apoptotic factor Bax,[12] we found that siRNA-mediated BCLAF1 knockdown led to suppressed Bax expression, which was highly induced by a high-dose IR, along with reduced activity of the Bax-downstream Caspase-9 and Caspase-3 as well as less cleaved PARP1 (a Caspase-3 substrate). These changes were more pronounced in IR-responsive cells than in IR-resistant cells (Figure 3e). These results collectively indicated that in IR-responsive cells, BCLAF1 has a pronounced role in disrupting the p21-dependent inhibition of activation of Caspase-dependent mitochondrial-mediated apoptotic pathways.

BCLAF1 is a regulator in the γH2AX-mediated repair of DNA DSBs. Based on our findings that BCLAF1 suppression is associated with both the H2AX-mediated p21-dependent cell cycle arrest and radio-resistance (Figure 3b), we reasoned that depending on the IR-responsive *versus* -resistant nature of the irradiated cells, BCLAF1 selectively regulates both γH2AX-mediated DDR associated with either apoptosis or DSB repair. We first investigated how BCLAF1 affects IR-induced formation of γH2AX foci, since such foci quantitatively correlate with the extent of DNA damage.[28] As shown in Figure 4a, the IR-resistant cancer cells contained much less DSB-indicative γH2AX and 53BP1 foci than those in the 10-Gy-irradiated IR-responsive cells, indicating attenuated DDR in tumor cells to repeated IR. BCLAF1

Figure 4 BCLAF1 regulates the subcellular-specific feedback loop in balancing apoptosis and cell cycle progression and DNA-PKcs regulates the formation of BCLAF1 foci. (**a**) Effect of BCLAF1 on the formation of DSB-indicative γH2AX and 53BP1 foci. A549 cells were harvested at 1 h after a defined IR and the percentage of γH2AX and 53BP1 foci-positive cells was determined by analyzing 100 randomly chosen cells and the number of γH2AX and 53BP1 foci per cell was determined on a cell-to-cell basis by the quantitative analysis of at least 30 cells randomly chosen as previously described.[32] Error bars represent S.D. of a technical duplicate. **$P<0.05$, *$P<0.01$. (**b**) Immunoblot analysis of the effect of BCLAF1 on Ku70 associations with DNA-PKcs in differentially irradiated A549 cells. Relative intensities representing the binding strength between DNA-PKcs and Ku70 measured by ImageJ (version 1.4.5q) are indicated as italic numbers. Data represent the average of two independent experiments. $P<0.05$. (**c**) The Ku70 immunoprecipitates were isolated from cytosolic and nuclear fractions of non-irradiated, IR-responsive, -resistant cells by using an agarose-conjugated Ku70 antibody. Individual complex components were immunoblotted with indicated antibodies. Relative intensities of interaction strength between DNA-PKcs, p18-cyclin E, Bax and Bcl-2, and Ku70 measured by ImageJ (version 1.4.5q) are indicated as italic numbers and separately measured for either nuclear or Cytosolic fraction. Data are from two independent experiments. $P<0.01$. (**d**) For each radiation condition without or with BCLAF1 knockdown, the cells were harvested after 1- or 8-h recovery time. Quantitative measurements of γH2AX were performed as described in the Materials and Methods section. One experiment containing a technical duplicate representative of two is shown with the data precision indicated by the error bar based on mean ± S.D. of duplicate samples. **$P<0.05$, *$P<0.01$. (**e**) Immunostaining of IR-induced BCLAF1 foci in the DNA-PKcs wild-type (*DNA-PKcs*^{+/−}) and null (*DNA-PKcs*^{−/−}) MEF cells under either IR-responsive or -resistant condition. DAPI was used to stain DNA. More than 200 cells from each condition were examined (scale bar is 8 μm)
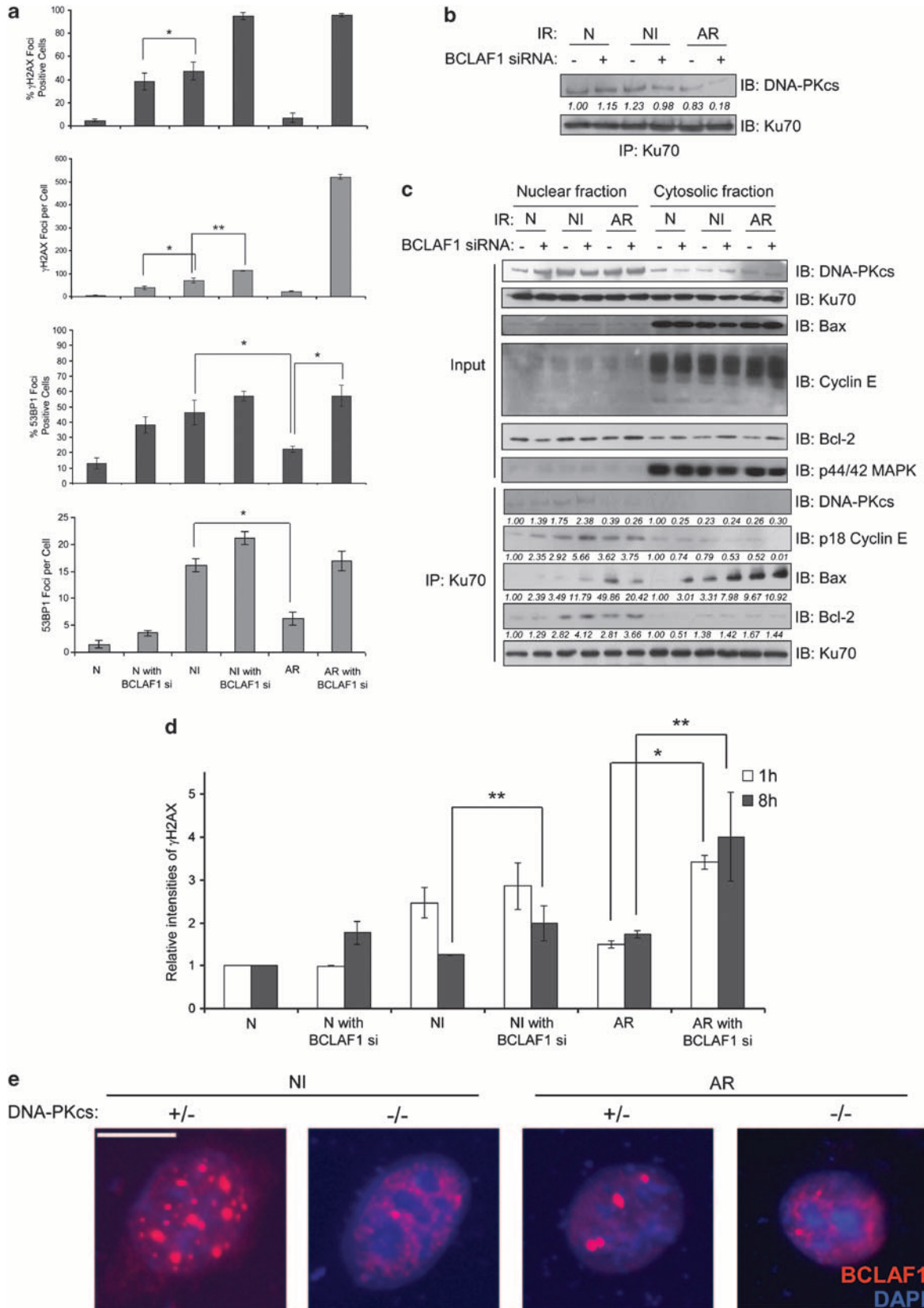
knockdown led to increased γH2AX and 53BP1 foci, surprisingly, more dramatically in IR-resistant than in IR-responsive cells. These results indicated that, first, BCLAF1 is actively involved in repairing DSBs to reduce γH2AX and 53BP1 foci in viable cells under IR-responsive condition. Second, suppressed BCLAF1 was accompanied either by more IR-resistant viable cancer cells with a larger population of persistently unrepaired DSBs probably at S phase (Figure 4a), or with deficient DNA repair,[29] all emphasizing that the central role of BCLAF1 in modulating diverse DDR, the regulation of DSB repair in particular.

BCLAF1 positively regulates both formation of the DNA-PK complex and the Ku70-mediated feedback loop. Our proteomics data showed the DNA-PK complex enhanced its interaction with γH2AX specifically in the 10-Gy-irradiated IR-responsive cells, whereas non-detectable interaction between γH2AX and ATM/ATR was found (Figure 1b and Supplementary Table S1). Previous work indicated that the formation of DNA-PK complex has a critical role in various H2AX-mediated DSB repair processes,[30] particularly through non-homologous end joining (NHEJ) occurring at the G_1/S transition, where Ku70 is a key regulator.[31] Further, BCL-2, which interacts with BCLAF1 *in vitro*[16] and negatively regulates DSB repair by disruption of the Ku/DNA-PKcs complex.[32] Based on these established links, we first examined whether BCLAF1 affects the integrity of this DNA-PK complex. In Ku70 immunoprecipitates from differentially irradiated cells, siRNA-mediated BCLAF1 knockdown generally led to a weakened association between Ku70 and DNA-PKcs, and to a greater extent in IR-resistant than in IR-responsive cells (Figure 4b), indicating that BCLAF1 positively regulates Ku70/DNA-PKcs-coordinated DSB repair through NHEJ.

Additionally, previous work indicated that Ku70 mediates a feedback loop selectively modulating the propensity toward apoptosis or cell cycle progression/survival.[33] In this loop, Caspase-3 activated by free Bax cleaves cyclin E to generate an 18-kDa C-terminal fragment, p18-cyclin E, which then complexes with cytosolic Ku70 to liberate the Ku70-bound Bax for inducing mitochondria-mediated apoptosis.[33,34] Based on our newly established links between BCLAF1 and major loop components, including Ku70, cyclin E, Bax, and Caspase-3 (Figures 3b and e), we then explored the function of BCLAF1 in this Ku70-mediated feedback loop by comparing the effect of BCLAF1 in formation of the Ku70 complexes under different radiation conditions. Because both cyclin E and DNA-PKcs are mainly localized in the nucleus, whereas Caspase-3 and Bax function in the cytoplasm,[30] our investigation was conducted with subcellular resolution. In nuclei of IR-responsive cells, BCLAF1 knockdown led to an increased association between Ku70 and p18-cyclin E (Figure 4c), indicating BCLAF1 may negatively regulate the DNA repair process mediated by the nuclear Ku70/p18-cyclin E complex,[33] promoting apoptosis. On the other hand, in the cytosol of BCLAF1-knockdown cells, Ku70 enhanced its binding to Bax but weakened its interaction with p18-cyclin E, suggesting that BCLAF1 is required to release Bax from the anti-apoptotic Ku70–Bax complex in high-dose-irradiated IR-responsive cells. Under IR-resistant condition, cytosolic

Ku70 formed a strong complex with Bax but weakened its interaction with p18-cyclin E, while BCLAF1 knockdown affected Ku70 binding to both proteins in a trend similar to wild-type cells (Figure 4c), indicating inhibition of apoptosis in the IR-resistant cancer cells is caused by the naturally suppressed BCLAF1. Further, BCLAF1 knockdown had little effect on the stability of the Ku70/p18-cyclin E complex in nuclei, suggesting a less active status of Ku-mediated DNA repair with already reduced BCLAF1. Coincidently, in the nuclear Ku70 complexes, BCL-2, showed similar changes in its affinity to Ku70 as to p18-Cyclin E (Figure 4c), indicating that, under IR-resistant condition with suppressed BCLAF1, p18-Cyclin E may cooperate with nuclear BCL-2 to suppress the NHEJ pathway for DNA repair.

Downregulation of endogenous BCLAF1 is associated with suppressed activity of NHEJ repair. Further, compared with 10-Gy-irradiated cells with a 1-h recovery, an approximately 50% reduction of γH2AX was observed in the IR-responsive cells recovered for 8 h, indicating activated DSB repair under IR-responsive condition (Figure 4d). However, less than 30% γH2AX reduction was found in similar IR-responsive cells with BCLAF1 knockdown. Under IR-resistant condition, neither a longer recovery time nor BCLAF1 knockdown had any impact on the amount of IR-induced γH2AX, probably due to already suppressed BCLAF1, all collectively confirming the regulatory role of BCLAF1 in NHEJ DNA repair.

DNA-PKcs regulates the formation/translocation of BCLAF1 foci. As DNA-PKcs phosphorylate many substrates involved in NHEJ-based DNA repair,[35] we investigated whether BCLAF1's DNA repair function could also depend on DNA-PKcs. In 10-Gy-irradiated *DNA-PKcs*$^{+/-}$ MEF cells, a large number of the IR-induced BCLAF1 foci were found widely distributed in nuclei, including some foci at the nuclear envelope, while few BCLAF1 foci were observed in the nucleoplasm of the 10-Gy-irradiated *DNA-PKcs*$^{-/-}$ MEFs (Figure 4e). In contrast, in both *DNA-PKcs*$^{+/-}$ and *DNA-PKcs*$^{-/-}$ MEFs under IR-resistant condition, the numbers of nuclear BCLAF1 foci were all reduced compared with those in IR-responsive cells (Figure 4e). Clearly, IR induction of BCLAF1 foci requires both DNA-PKcs and cellular sensitivity to radiation. Further, through tandem mass spectrometry experiments, a predominant phosphoserine at 151 with a phosphotyrosine at 150 were unambiguously identified at BCLAF1 isolated from 10-Gy-irradiated *DNA-PKcs*$^{+/-}$ or *DNA-PKcs*$^{-/-}$ MEFs (Supplementary Figure 6). However, compared with that originated from irradiated *DNA-PKcs*$^{-/-}$ cells, the phosphorylation level of serine 151 at BCLAF1 isolated from wild-type *DNA-PKcs*$^{+/-}$ MEFs showed an approximately 30% increase in site occupancy determined by our newly developed label-free quantitation method using peak area and spectral counting (Supplementary Figures 7 and 8). Given that serine 151 is located in an RS domain, and such domains are known to regulate subcellular localization[36] (Supplementary Table S4), these quantitative MS results suggested that, stimulated by high-dose IR, DNA-PKcs drives BCLAF1 to the nuclear envelope by directly phosphorylating key BCLAF1 RS residue(s). Based on our observations that γH2AX could be

co-localized with not only BCLAF1 (Figure 1d) but also activated DNA-PKcs in the nuclei of 10-Gy-irradiated IR-responsive cells, BCLAF1 may also co-localize with DNA-PKcs at the same nuclear location, defining it as a DNA-PK-dependent NHEJ repair protein.

Discussion

Although growing numbers of H2AX interactors involving diverse biological processes have been identified, for cells showing different sensitivities to radiation, it is still incomplete as to how exactly H2AX coordinates specific pathways for different cell fates and what co-factors are involved in these pathways. Strategically, not starting with pre-conceived notions, we first conducted a phenotype-specific dissection of IR-induced H2AX-interacting protein network and then performed zoom-in characterization of novel H2AX partners, their H2AX-coordinated interplay on a pathway scale in particular. Technically, by integrating the results from multiple approaches of quantitative proteomics, cell biology,

immunoblotting and confocal imaging, we revealed a mechanistic view that in diverse γH2AX-dependent cell fate-determining pathways, an IR-inducible H2AX-associating partner, BCLAF1, has diverse roles in regulating either apoptosis, or cell survival with active DNA repair or carcinogenesis (Figure 5).

Given that depletion of Bcl-2 could enhance the DNA-binding activity of the Ku70/DNA-PKcs complex for accelerating DNA repair,[32] our finding that BCLAF1 knockdown causes a reduced association between Ku70 and DNA-PKcs (Figure 4b) implied that BCLAF1 is required for stability of the DNA-PK complex critical for NHEJ DSB repair. Mechanistically, in the γH2AX interactome induced by a high-dose acute IR, DNA-PKcs is activated to phosphorylate both H2AX and BCLAF1 resulting in the translocation of some BCLAF1 to γH2AX foci in nuclei, where BCLAF1 serves as an inducer for a p53-dependent G_2/M arrest of irreparable cells as well as a positive regulator of DNA-PK-dependent DNA repair in the surviving cells with DSBs (Figure 5). Meanwhile, the remaining BCLAF1 in cytosol is required for the pro-apoptotic side of
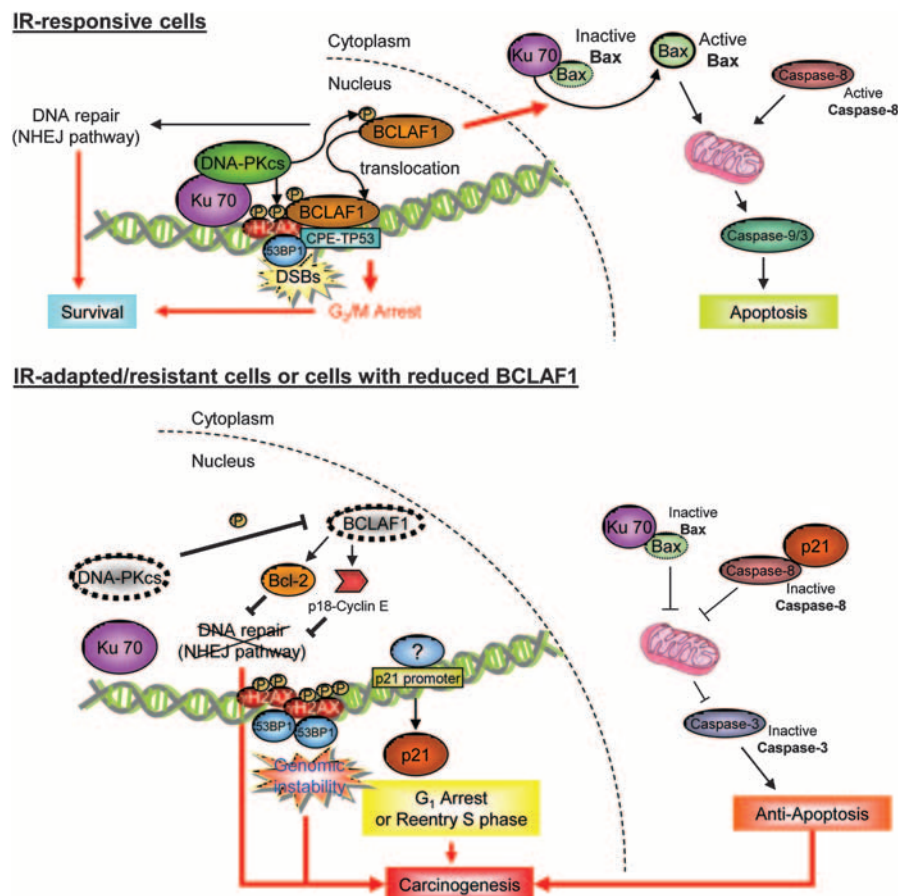

Figure 5 A mechanistic model illustrating the multiple roles of BCLAF1 in regulation of apoptosis, cell cycle progression, and NHEJ DBS repair. In IR-responsive cells exposed to a high-dose radiation that activates DNA-PKcs, BCLAF1 re-localizes to the nuclear envelope through site-specific phosphorylation by DNA-PKcs and then emerges with γH2AX foci, which in turn stabilizes the Ku70/DNA-PKcs complex for facilitating NHEJ DSB repair. Meanwhile, BCLAF1 regulates both cyclin E and p53/p21-dependent mitochondria-mediated pathway(s) for promoting pro-apoptotic activity of Caspase-3, leading to the generation of an apoptotic amplifier, p18-cyclin E, followed by Ku70-mediated liberation of active Bax. In contrast, in the IR-resistant carcinoma cells BCLAF1 is intrinsically suppressed, leading to weakened Ku70/DNA-PKcs complex but enhanced associations of Ku70/BCL-2/p18-Cyclin E instead, subsequently reducing the activity of DSB repair. In the cytosol, suppressed BCLAF1 could result in more Ku70-bound Bax, which inhibits the formation of pro-apoptotic Ku70-p18-Cyclin E complex

Ku70-mediated feedback loop where BCLAF1 promotes Caspase-3-mediated cleavage of cyclin E, and subsequently induces the dissociation of Bax from its complex with Ku70 for the activation of pro-apoptotic Bax.

On the other hand, BCLAF1 was found intrinsically suppressed in tumor cells with natural radio-resistance. Similar to the effects of siRNA-mediated BCLAF1 knockdown, the suppressed BCLAF1 corresponds to less-translocated BCLAF1 in nuclei, affecting the stability of the Ku70/DNA-PKcs complex for reduced DNA repair, leading to p21-dependent cell arrest at G_1 phase or reentry to S phase with replicating the errors caused by DSBs. Meanwhile, with less BCLAF1 modulation, the Ku70-mediated Caspase-dependent mitochondrial-mediated apoptotic pathways could be inhibited for developing apoptosis resistance in mis-replicated surviving cells, eventually leading to carcinogenesis. We therefore concluded that BCLAF1 is a γH2AX-dependent tumor suppressor.

On a systems view, our combined results reveals that cell fate decision is made by the γH2AX-coordinated network specifically involving BCLAF1 and DNA-PKcs, illustrating how the balance between tissue protection from repetitive challenges and eliminating irreparable DSBs could be tightly regulated, or altered, or abrogated based on the extent of DNA damage.

Materials and Methods

Cell lines, reagents, and AACT/SILAC labeling. Human embryonic kidney (HEK) 293T, normal human fibroblast strains (MRC-5 and WI-38), human osteosarcoma strain (U-2 OS), human lung adenocarcinoma cell line A549, and p53-deficient lung carcinoma H1299 cells were purchased from ATCC (Manassas, VA, USA) and DNA-PKcs wild-type (*DNA-PKcs$^{+/-}$*) and null (*DNA-PKcs$^{-/-}$*) MEF cells were kindly provided by Dr. David J Chen. A 293T cell line stably expressing FLAG-tagged H2AX (FLAG-H2AX) was established as described previously.[7] 293T, *DNA-PKcs$^{+/-}$* and *DNA-PKcs$^{-/-}$* MEF cells, A549 and H1299 cells were maintained in D-MEM supplemented with 10% FBS, 1% penicillin and streptomycin, U-2 OS cells were grown in McCoy's 5a with 10% FBS, 1% penicillin, and streptomycin, and MRC-5 and WI-38 cells were in MEM with 10% FBS, 1% penicillin, and streptomycin, 0.1 mM NEAA and 1 mM sodium pyruvate (Invitrogen, Carlsbad, CA, USA). For AACT labeling, the FLAG-H2AX cells were grown in media supplemented with either L-$^{12}C_6$-arginine ('light'), or L-$^{13}C_6$-arginine ('medium'), or L-$^{13}C_6$, $^{15}N_4$-Arginine ('heavy') (Cambridge Isotope Laboratories, Andover, MA, USA), respectively. siRNA duplexes targeting BCLAF1 were synthesized and purified by Sigma (St. Louis, MO, USA) (MISSION siRNA) and transfected with Lipofectamine RNAiMAX (Invitrogen). The following siRNA sequences were used: *BCLAF1* #1, 5′-CAAGAAUUCCGAUCCAUCU-3′; #2, 5′-AGAUGGAUCGGAAUUCUUG-3′.

Radiation treatment and H2AX immunoprecipitation. Stable cells incorporating $^{13}C_6$-Arg or $^{13}C_6^{15}N_4$-Arg tags were exposed to a γ-ray (AECL Gammacell 40 Irradiator) at 7.5 cGy or 10 Gy, respectively, at the dose rate of 0.75 Gy min^{-1} followed by 1 h recovery. Approximately 8×10^8 cells of each type were harvested and H2AX complexes were immunoprecipitated as previously described.[7]

Mass spectrometry. IP elutes were separated on NuPAGE 4–12% bis-tris gel (Invitrogen). After staining with Coomassie Brilliant Blue, the entire gel lane was cut into contiguous 22 slices. In-gel digestion was performed on each gel slice and the mixture of peptide digests was extracted from gel. For LC-MS/MS analysis, each peptide set was desalted using the house-made C_{18} STAGE tips,[37] and then separated with on-line Eksigent nanoLC system coupled to an LTQ-Orbitrap hybrid mass spectrometer (Thermo Electron, San Jose, CA, USA) which is equipped with a nano-electrospray source (New Objective, Inc., Woburn, MA, USA). The peptides were first loaded on IntegraFrit trapping column (ProteoPep II

C18, 300 Å, 5 μm, 100 μm × 25 mm, New Objective, Inc.) by using mobile phase of 5% acetonitrile (ACN) in 0.1% formic acid (FA). The retained peptides were washed with the same buffer and were separated on a PicoFrit Analytical Columns (ProteoPep II C18, 300 Å, 5 μm, 50 μm × 100 mm, tip ID = 10 μm, New Objective, Inc.) by applying a multistep gradient of ACN (5% A in 5 min, 5–40% A in 40 min, 40-90% A in 70 min, isocratic gradient 5 min at 90%, 90-5% A in 95 min; solvent A: 0.1% FA; solvent B: 0.1% FA in 95% ACN). The set of MS/MS raw data first converted to DTA files using ThermoElectron Bioworks 3.3.1 was searched against the IPI-human Fasta database using SEQUEST. The parameters for data search included (1) variable modifications allowing mass difference of 80 Da for possible phophorylation and 6, or 10 Da for $^{13}C_6$-Arg, or $^{13}C_6$, $^{15}N_4$-Arg, respectively, (2) tryptic peptides with allowance of two missed cleavages, and (3) top hit(s) with individual cross-correlation over the threshold dependent on precursor charge states. The proteins with at least two peptides detected ($P < 0.05$) were considered as positive identifications. PepQuan software was used for AACT/SILAC-based peptide/protein quantification.

AACT-based quantitation for distinguishing dose-dependent H2AX interactors. For each arginine-containing peptide, a set of three isotope signals spacing by 6 Da and 10 Da were observed as the 'light (L)' isotope peak was originally from the non-irradiated cells, and the 6 Da (M) or 10 Da (H) signals came from the cells irradiated by IR at 7.5 cGy or 10 Gy, respectively. The ratio of any paired heavy *versus* light isotope signals, that is, M/L or H/L, was then correlated with the IR-induced dose-dependent abundance of individual protein bound to H2AX (bait) (Figure 1b). With respect to the relative abundance of H2AX in the immunoprecipitate mixture, which was found to be equal at 1 : 1 : 1, we have set a quantitative threshold to distinguish those IR-inducible/induced H2AX-interacting partners from non-specific background. In reference to the criteria previously established by our group,[38] we first found the average relative S.D. (RSD) for quantitative measurements of M/L or H/L ratio was at 8.9% and then used three-fold RSD, which was approximately equal to 30% changes in the H2AX-bound abundances as the threshold. For most of non-specific contaminants, their M/L or H/L ratios were close to a unity because of their possibly equal distribution in each immunoprecipitate, for example, hnRNPA1, any identified protein with H/L larger than 1.3 or less than 0.7 was indicative of that its association with H2AX was enhanced or weakened upon the radiation at defined dose level.

Label-free quantitation. Label-free quantitation was performed using MS1 peak area as described previously,[39] and total protein quantitation based on MS2 spectral counting was performed via ProteoIQ label-free quantitation software (NuSep, Bogart, GA, USA).

Bioinformatics analysis. PANTHER (http://www.pantherdb.org) and DAVID (http://david.abcc.ncifcrf.gov/) were used to analyze the functional category of the identified proteins. Domain analysis was performed by using similar hierarchical clustering approach[13] with modifications: both interaction and functional domains in each H2AX-binding protein were identified by SMART (Simple Modular Architecture Research Tool) and Pfam (Protein Family Database). A statistical algorithm based on the average-linkage method was used to establish a similarity metric that relates proteins based on the correlation coefficient of their domains, and *vice versa*. The cluster file was loaded onto Treeview (version 1.60; http://rana.lbl.gov/EisenSoftware.htm) to generate a 2D branched-tree image including the phylogenic order of proteins and domain entries.

Co-immunoprecipitation and immunoblotting. Nuclear extracts and immunoprecipitates were obtained, separated, and transferred as described previously,[7] The PVDF membranes (Bio-Rad, Hercules, CA, USA) were blotted respectively with a rabbit polyclonal antibody against BCLAF1 (A300-608A, BETHYL laboratories, Inc., Montgomery, TX, USA), and Histone H3S10ph (ab47297, Abcam, Cambridge, MA, USA), and DNA-PKcs (4602), cleaved Caspase-3 (Asp175) (9664), Caspase 8 (4927) and Bax (2772) (Cell Signaling Technology, Danvers, MA, USA) and Cyclin D1 (H-295) (sc-753) (Santa Cruz Biotechnology, Inc., Santa Cruz, CA, USA); goat-polyclonal antibody against β-actin (sc-1615) (Santa Cruz Biotechnology, Inc.) and GAPDH (IMG-3073) (Imgenex Inc., San Diego, CA, USA); mouse monoclonal antibody against FLAG M2 (F1804), BrdU (B8434) and p21 (P1484) (Sigma), γH2AX (ab22551) (Abcam) and, PARP1 (sc-8007), p53 (DO-1) (sc-126), Bcl-2 (C-2) (sc-7382) and Ku70

(N3H10) (sc-56129) (Santa Cruz Biotechnology, Inc.) and Caspase-9 (9508) (Cell Signaling Technology) and Cyclin E (Ab-2) (MS-870-P0) (Thermo Scientific, Inc., Waltham, MA, USA) and 53BP1 (612522) (BD, San Jose, CA, USA). The membranes were incubated with anti-rabbit (Thermo Scientific), anti-mouse (Bio-Rad) or anti-goat (Invitrogen) immunoglobulin G-peroxidase conjugate and visualized by using an 'ECL plus' detection kit (GE Healthcare, Waukesha, WI, USA). The levels of Cyclins D1 and E and γH2AX proteins from immunoblotting assays were quantified by densitometry with ImageJ software.

Immunofluorescence assay. Cells were grown on coverslips, irradiated, washed with PBS, fixed with 4% formaldehyde, and permeabilized with 0.1% NP-40 for 5 min at room temperature. The cells were then incubated in blocking buffer (PBS containing 3% BSA) for 30 min, followed by incubation with the primary antibody (anti-γH2AX antibody or anti-53BP1 antibody or anti-BCLAF1 antibody for co-localization assay; anti-BrdU or anti-Histone H3S10ph for cell cycle assay), and blocking with 1% BSA in PBS for 1 h. Following PBS washing, the cells were incubated with secondary antibody (Alexa-488-conjugated anti-mouse IgG or Alexa-568-conjugated anti-rabbit IgG (Molecular Probes, Life Technologies, Grand Island, NY, USA) for 1 h. Following a wash with PBS-containing 4,6-diamidino-2-phenylindole (DAPI; Invitrogen), coverslips were mounted onto glass slides using Permount solution (Fisher Scientific, Pittsburgh, PA, USA). Confocal laser scanning microscopy was performed on a LeicaSP2 AOBS Upright laser scanning confocal microscope using the 354-nm line of a UV laser and the 488- and 568-nm lines of argon and helium-neon lasers. The images were processed using LCS Lite software (Leica, Buffalo Grove, IL, USA).

Semi-quantitative RT-PCR analysis. Total RNA (approximately 2 μg) was isolated by using RNeasy spin column kits (Qiagen, Valencia, CA, USA), and then reverse transcribed into cDNA by using Superscript II reverse-transcriptase (Invitrogen) at 50 °C. Control reactions were performed without template RNA and Superscript II or with no template cDNA. PCR reactions were done with the cDNA generated from 500 ng of total RNA in a 25-μl reaction, in triplicate for each sample. Both p53 and β-actin were amplified by described primer sets.[40]

Chromatin immunoprecipitation (ChIP) assay. IR-treated cells were cross-linked at 80% to 90% confluence with 1% formaldehyde, incubated for 15 minutes and then quenched with 0.1 M glycine-PBS for 5 minutes. The collected cells were washed with 50 mM glycine-PBS and harvested. Each ChIP was performed using SimpleChIP Enzymatic Chromatin IP Kit (Cell Signaling). In all, 2% of the cellular extract before immunoprecipitation was used for the input control. DNA was purified by DNA Purification Columns (Cell Signaling). PCR amplification was performed in ChIP fragments using the oligonucleotide sequences described previously.[11]

Conflict of Interest
The authors declare no conflict of interest.

1. Lobrich M, Jeggo PA. The impact of a negligent G2/M checkpoint on genomic instability and cancer induction. *Nat Rev Cancer* 2007; **7**: 861–869.
2. Zhou H, Randers-Pehrson G, Geard CR, Brenner DJ, Hall EJ, Hei TK *et al*. Interaction between radiation-induced adaptive response and bystander mutagenesis in mammalian cells. *Radiat Res* 2003; **160**: 512–516.
3. Bonner WM, Redon CE, Dickey JS, Nakamura AJ, Sedelnikova OA, Solier S *et al*. γH2AX and cancer. *Nat Rev Cancer* 2008; **8**: 957–967.
4. Paulsen RD, Soni DV, Wollman R, Hahn AT, Yee MC, Guan A *et al*. A genome-wide siRNA screen reveals diverse cellular processes and pathways that mediate genome stability. *Mol Cell* 2009; **35**: 228–239.
5. Chen X, Smith LM, Bradbury EM. Site-specific mass tagging with stable isotopes in proteins for accurate and efficient protein identification. *Anal Chem* 2000; **72**: 1134–1143.
6. Wang T, Gu S, Ronni T, Du YC, Chen X. In vivo dual-tagging proteomic approach in studying signaling pathways in immune response. *J Proteome Res* 2005; **4**: 941–949.
7. Du Y-C, Gu S, Zhou J, Wang T, Cai H, Macinnes MA *et al*. The dynamic alterations of H2AX complex during DNA repair detected by a proteomic approach reveal the critical roles of Ca2 + /calmodulin in the ionizing radiation-induced cell cycle arrest. *Mol Cell Proteomics* 2006; **5**: 1033–1044.
8. Heo K, Kim H, Choi SH, Choi J, Kim K, Gu J *et al*. FACT-mediated exchange of histone variant H2AX regulated by phosphorylation of H2AX and ADP-ribosylation of Spt16. *Mol Cell* 2008; **30**: 86–97.
9. Xiao A, Li H, Shechter D, Ahn SH, Fabrizio LA, Erdjument-Bromage H *et al*. WSTF regulates the H2A.X DNA damage response via a novel tyrosine kinase activity. *Nature* 2009; **457**: 57–62.
10. Cook PJ, Ju BG, Telese F, Wang X, Glass CK, Rosenfeld MG *et al*. Tyrosine dephosphorylation of H2AX modulates apoptosis and survival decisions. *Nature* 2009; **458**: 591–596.
11. Liu H, Lu Z-G, Miki Y, Yoshida K. Protein kinase C {delta} induces transcription of the TP53 tumor suppressor gene by controlling death-promoting factor Btf in the apoptotic response to DNA damage. *Mol Cell Biol* 2007; **27**: 8480–8491.
12. Sarras H, Alizadeh Azami S, McPherson JP. In search of a function for BCLAF1. *Scientific World J* 2010; **10**: 1450–1461.
13. Eisen MB, Spellman PT, Brown PO, Botstein D. Cluster analysis and display of genome-wide expression patterns. *Proc Natl Acad Sci USA* 1998; **95**: 14863–14868.
14. Kruse J-P, Gu W. Modes of p53 Regulation. *Cell* 2009; **137**: 609–622.
15. Meek DW. Tumour suppression by p53: a role for the DNA damage response? *Nat Rev Cancer* 2009; **9**: 714–723.
16. Kasof GM, Goyal L, White E. Btf, a novel death-promoting transcriptional repressor that interacts with Bcl-2-related proteins. *Mol Cell Biol* 1999; **19**: 4390–4404.
17. Haraguchi T, Holaska JM, Yamane M, Koujin T, Hashiguchi N, Mori C *et al*. Emerin binding to Btf, a death-promoting transcriptional repressor, is disrupted by a missense mutation that causes Emery-Dreifuss muscular dystrophy. *Eur J Biochem* 2004; **271**: 1035–1045.
18. Oberdoerffer P, Sinclair DA. The role of nuclear architecture in genomic instability and ageing. *Nat Rev Mol Cell Biol* 2007; **8**: 692–702.
19. Fragkos M, Jurvansuu J, Beard P. H2AX is required for cell cycle arrest via the p53/p21 pathway. *Mol Cell Biol* 2009; **29**: 2828–2840.
20. Murray AW. Recycling the cell cycle: cyclins revisited. *Cell* 2004; **116**: 221–234.
21. Bracken CP, Wall SJ, Barré B, Panov KI, Ajuh PM, Perkins ND *et al*. Regulation of cyclin D1 RNA stability by SNIP1. *Cancer Res* 2008; **68**: 7621–7628.
22. Abbas T, Dutta A. p21 in cancer: intricate networks and multiple activities. *Nat Rev Cancer* 2009; **9**: 400–414.
23. McPherson JP, Sarras H, Lemmers B, Tamblyn L, Migon E, Matysiak-Zablocki E *et al*. Essential role for Bclaf1 in lung development and immune system function. *Cell Death Differ* 2009; **16**: 331–339.
24. Nishizaki M, Meyn RE, Levy LB, Atkinson EN, White RA, Roth JA *et al*. Synergistic inhibition of human lung cancer cell growth by adenovirus-mediated wild-type p53 gene transfer in combination with docetaxel and radiation therapeutics in vitro and in vivo. *Clin Cancer Resh* 2001; **7**: 2887–2897.
25. Olive PL, Durand RE. Drug and radiation resistance in spheroids: cell contact and kinetics. *Cancer Metastasis Rev* 1994; **13**: 121–138.
26. Maity A, McKenna WG, Muschel RJ. The molecular basis for cell cycle delays following ionizing radiation: a review. *Radiotherapy Oncol* 1994; **31**: 1–13.
27. Coqueret O. New roles for p21 and p27 cell-cycle inhibitors: a function for each cell compartment? *Trend Cell Biol* 2003; **13**: 65–70.
28. Rogakou EP, Boon C, Redon C, Bonner WM. Megabase chromatin domains involved in DNA double-strand breaks in vivo. *J Cell Biol* 1999; **146**: 905–916.
29. Kuhne M, Riballo E, Rief N, Rothkamm K, Jeggo PA, Löbrich M *et al*. A double-strand break repair defect in ATM-deficient cells contributes to radiosensitivity. *Cancer Res* 2004; **64**: 500–508.
30. Downs JA, Jackson SP. A means to a DNA end: the many roles of Ku. *Nat Rev Mol Cell Biol* 2004; **5**: 367–378.
31. Hakem R. DNA-damage repair; the good, the bad, and the ugly. *EMBO J* 2008; **27**: 589–605.
32. Wang Q, Gao F, May WS, Zhang Y, Flagg T, Deng X *et al*. Bcl2 negatively regulates DNA double-strand-break repair through a nonhomologous end-joining pathway. *Mol Cell* 2008; **29**: 488–498.
33. Mazumder S, Plesca D, Almasan A. A jekyll and hyde role of cyclin E in the genotoxic stress response: switching from cell cycle control to apoptosis regulation. *Cell Cycle* 2007; **6**: 1437–1442.
34. Mazumder S, Gong B, Chen C, Drazba J, Buchsbaum J, Almasan A. Proteolytic cleavage of cyclin E leads to inactivation of associated kinase activity and amplification of apoptosis in hematopoietic cells. *Mol Cell Biol* 2002; **22**: 2398–2409.
35. Lieber MR. The mechanism of double-strand DNA break repair by the nonhomologous DNA end-joining pathway. *Annu Rev Biochem* 2010; **79**: 181–211.

36. Long JC, Caceres JF. The SR protein family of splicing factors: master regulators of gene expression. *Biochem J* 2009; **417**: 15–27.

37. Rappsilber J, Mann M, Ishihama Y. Protocol for micro-purification, enrichment, pre-fractionation and storage of peptides for proteomics using StageTips. *Nat Protocols* 2007; **2**: 1896–1906.

38. Xue Y, Yun D, Esmon A, Zou P, Zuo S, Yu Y *et al.* Proteomic dissection of agonist-specific TLR-mediated inflammatory responses on macrophages at subcellular resolution. *J Proteome Res* 2008; **7**: 3180–3193.

39. Gunawardena HP, Huang Y, Kenjale R, Wang H, Xie L, Chen X *et al.* Unambiguous characterization of site-specific phosphorylation of leucine-rich repeat Fli-I-interacting protein 2 (LRRFIP2) in toll-like receptor 4 (TLR4)-mediated signaling. *J Biol Chem* **286**: 10897–10910.

40. Avery-Kiejda KA, Zhang XD, Adams LJ, Scott RJ, Vojtesek B, Lane DP *et al.* Small molecular weight variants of p53 are expressed in human melanoma cells and are induced by the DNA-damaging agent cisplatin. *Clin Cancer Res* 2008; **14**: 1659–1668.

Supplementary Information accompanies the paper on Cell Death and Disease website (http://www.nature.com/cddis)